Bragg-Fresnel Optics at the ESRF: microdiffraction and microimaging applications

Anatoly Snigirev
European Synchrotron Radiation Facility, B.P. 220, F38043 Grenoble Cedex, France

Victor Kohn
Russian Research Centre "Kurchatov Institute", 123182 Moscow, Russia

ABSTRACT

Bragg-Fresnel Optics shows excellent compatibility with ESRF sources and is capable of obtaining monochromatic submicron focal spots with 10^8-10^9 photons/sec in an energy bandwidth of 10^{-4}-10^{-6} and in a photon energy range between 2-100keV. Microprobe and microimaging techniques based on Bragg-Fresnel optics were realised at the ESRF beamlines.

Key words: Bragg-Fresnel optics, x-ray microbeams, x-ray microscopy, microdiffraction, microfluorescence.

1. INTRODUCTION

It is no overestimation to state, that high energy x-ray microbeam and microimaging technology is concentrated at the third generation synchrotron radiation machines such as ESRF, APS and Spring-8, and in the future this will become even more evident, especially if we are talking about submicrometer resolution. In addition to a beam of extremely high brilliance, these x-ray sources are characterized by very small source size. A typical source size at the ESRF is 50-100μm, that at the source -to-sample distance of 50 m gives an angular source aperture of about 1-2μrad. Evidently, this level of the beam coherence imposes special requirements on the optics to be installed at the beamlines. The coherence preservation is precisely, an essential feature which is required of the optics. It would seem that only crystal optics based on perfect single crystals can meet these requirements. Moreover, an energy range of 2 to 100keV is covered just by Bragg diffraction crystal optics. However, experience shows, there is a fundamental resolution limit for crystal focusing optics, owing to the extinction depth of Bragg reflection, that is about 2-10μm. This limit can be overcome by the implementation of Fresnel diffraction along with Bragg reflection. This is precisely the main concept of Bragg-Fresnel Optics (BFO).

2. BRAGG-FRESNEL CRYSTAL OPTICS

2.1. Basic principles and properties of BFO.

BFO was put forward in the Institute of Microelectronics Technology Russian Academy of Sciences ten years ago[1]. Since that time a lot of efforts has been spent on both BFO technology development and on experimental and theoretical research on the BFO performance[2-6]. Bragg-Fresnel crystal optics is based on a superposition of Bragg diffraction by a crystal and dispersion by a Fresnel structure, which is patterned on the surface or grooved into the crystal. Unlike the transmission FZP the Bragg-Fresnel lens (BFL) is working in reflection. Its main advantage is that the various possibilities of beam transformation arising from the specific properties of Fresnel structures now become accessible to the high energy x-ray range.

It is clear that in general Fresnel zone structure on the surface of the flat crystal has an elliptical shape. Fig.1 demonstrates an elliptical BFL with a gold mask. This type of BFL acts as an amplitude zone plate. In addition to low

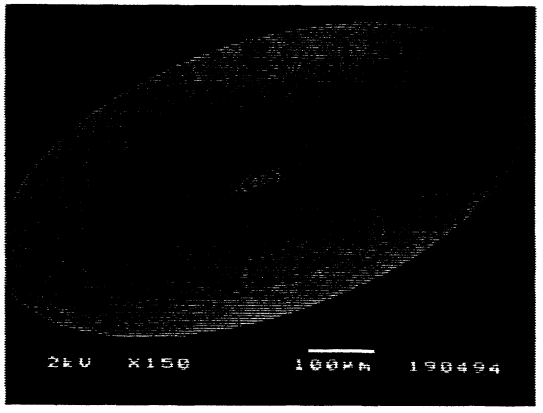

Fig.1 Elliptical amplitude BFL with the gold mask

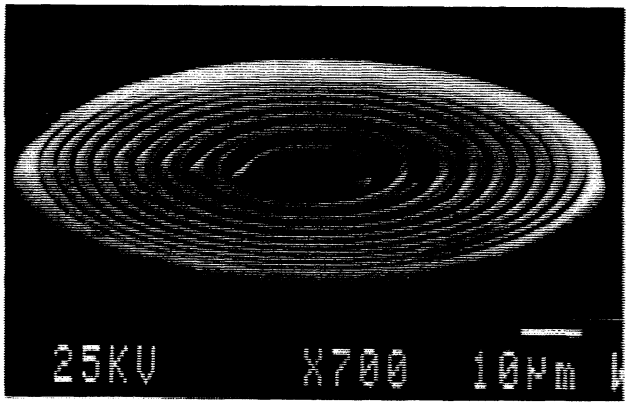

Fig.2 Elliptical Si-based BFL with slope zones

efficiency (~10%) and an existence of zero order of diffraction, relatively thick gold profile (few microns) creates some shadowing effect in the diffraction plane, that courses significant resolution lost. Considering Bragg-Fresnel lens as a holographic optical element with three dimensional zone structure a remarkable study was done on BFL with the slope zones[7]. One of the example of the elliptical BFL with the inclined profile is shown in Fig.2. Unfortunately, all attempts to obtained reasonable BFL focusing properties failed. Apparently further optimization of the profile structure is needed.

It turned out that linear and circular BFLs with rectangular profile are ideal for practical applications (Fig.3-4). In this case sagittal and backscattering geometries for linear[8] and circular[9] BFLs are respectively applied. The wave reflected by the lower surface of the BFL zone structure gains an additional phase shift π, as compared to that reflected by the upper surface. So far BFL is a purely phase element, since upon diffraction of the x-ray wave on the BFL zone structure no amplitude modulation

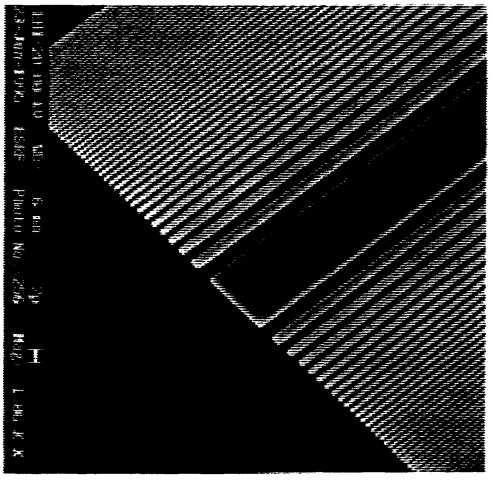

Fig.3 Linear Si-based BFL

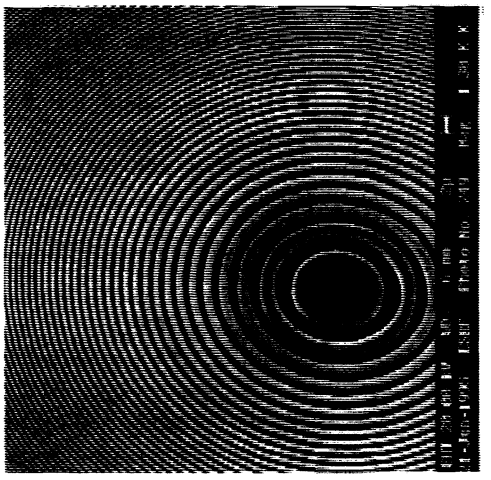

Fig.4 Circular Ge-based BFL

of the reflected wave is observed. Moreover BFL phase shift for a certain reflection is independent on the energy and is determined by the structure height only[8]. Diffraction efficiency of the BFL is very closed to the theoretical performance and is about 40% . The limiting spatial resolution that can be obtained in BFO is given by the width of the outermost zone of the zone structure. Present technologies permit to achieve fractions of a micron.

The focusing properties of linear Bragg-Fresnel lens do not depend on the energy and the same BFL can be used for a wide energy range determined by a Bragg reflection only. Tests of linear BFL were done at the undulator source and wiggler sources. It was shown that linear BFL is capable of focusing white radiation in the range from 2 to 100keV. Focus spot about 1-5μm has been observed and was limited by the source size according the demagnification ratio.

A limitation of the one dimensional focusing by linear BFL can be easily overcome by applying Kirckpatrick-Baez geometry[10,11] or cylindrical bending of the BFL (Fig.5). Experiment on curved BFL has been successfully done at the Optics Beamline. Focus spot of about $3*8\mu m^2$ has been measured at 20keV energy and the gain in the flux more than 100 compare with the flat BFL has been achieved[12].

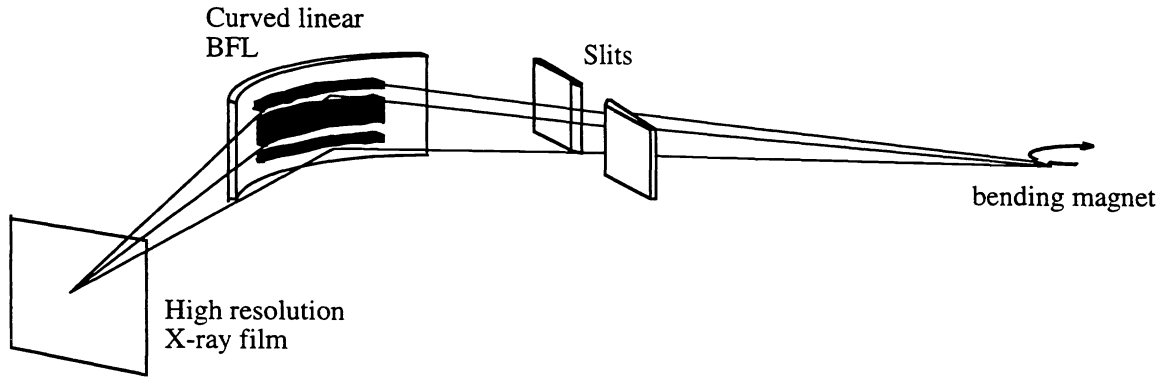

Fig.5 Experimental layout for BFL bending.

Systematic measurement of the optical properties of the circular BFL was done at different energies and gap settings of the high-β undulator. It was shown that the imaging can be made with significant diffraction efficiency of the BFL in the energy range of about 2keV-18keV when the reflections were varied from Si-111 to Si-999

3. APPLICATIONS.

It is evident that a combination of microfocusing x-ray optics with the high brilliance x-ray beams provided by the third generation synchrotron radiation sources like ESRF opens up new capabilities to develop hard x-ray microimaging and microprobe techniques [13-23,27].

3.1. Microfluorescence

A varied program of experiments using X-ray microbeam fluorescence as a means of characterization materials on the micrometer and sub-micrometer scales was carried out. The experiments have been performed at different undulator and bending magnet beamlines at the ESRF. Fluorescence microprobes based on linear and circular crystal BFL were tested[15,16]. The focal spot of 0.8μm with intensity 10^8 - 10^9 photons/sec for linear BFL and 0.7 microns with intensity 10^7 - 10^8 for circular BFL was achieved for undulator beamline. For the elliptical multilayer BFL[17] the focal spot around 2-3 microns with intensity 10^8 - 10^9 photons/sec was shown at the bending magnet and therefore the flux of about 10^{10} - 10^{11} photons/sec seems to be achievable at the undulator source. Applications of the developed fluorescence microprobes for elemental distributions in volcanic rocks, Antarctica micrometeorites, bone specimens and human hair slices were demonstrated.

3.2. Microdiffraction

3.2.1. SAXS camera

The attractive feature of proposed BFL-based camera is the fact that one can measure down to the smallest angles without using a complicated collimation system: defining and guard apertures (slits). The performance of the BFL-based SAXS camera has been designed and tested at the Microfocus beamline[18].

Schematic layout of this camera is presented in Fig.6. The 10keV monochromatic beam was focused on a sample by a circular Bragg-Fresnel lens using the 555-reflection in nearly backscattering geometry. The focused beam spot of about $1.5*2\mu m^2$ had

the intensity of the order of 10^8ph/s. The angular resolution of SAXS camera is defined by the divergence of the beam at the sample and is equal to the ratio of the BFL aperture (A=200μm) to the focal distance (F=0.62m): A/F=3*10^4 radian, that means the samples with the spacings less than 3000Å - 4000Å can be studied using the proposed camera. The diffraction patterns from the turkey tendon collagen were detected on the Molecular Dynamics image plate. The first 25 meridional reflections were resolved. Thus, small-angle scattering is possible from a sample on the scale of a few μm and can be extended to the subμm range. These open the possibility for new applications of SAXS, in particular in the area of surfaces and interfaces.

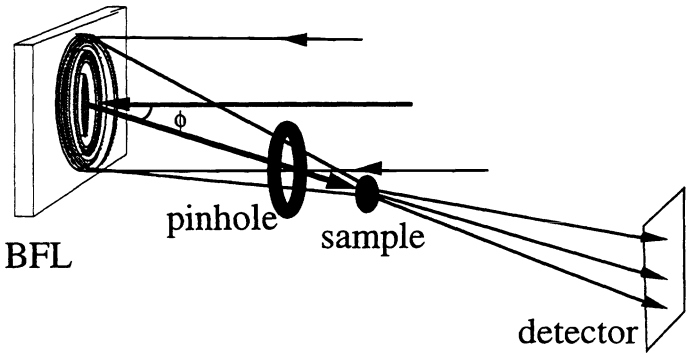

Fig.6 Schematic layout of the optical principle of the BFL-based SAXS camera

2.2.2. High pressure diffraction

It is evident that microbeam is very desirable for high pressure experiments, especially when diamond cells have to be transparent for x-rays and very little amount of sample is involved in the measurement[19]. The experimental setup is illustrated in Fig.7. The BFL structure was illuminated with a 0.2*0.15mm^2 beam from the undulator. A 26keV monochromatic beam was selected from the 10th harmonic at a Bragg angle of 4.4° and vertically focused by the lens into a narrow line on the gasket hole. Image plates were located 260 to 320 mm from the cell depending on the sample studied. A range of samples were investigated, but more important results were obtained on oxygen at very high pressures (up to 108GPa).

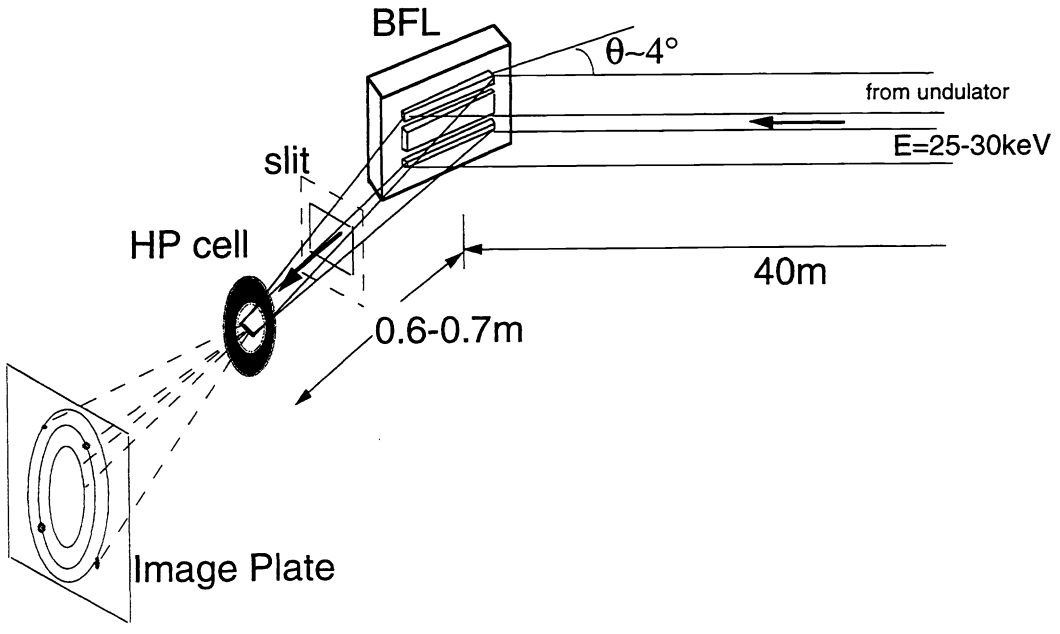

Fig.7 Experimental setup for high pressure studies.

2.2.2. High resolution diffraction - multicrystal diffractometry

Single crystal Bragg-Fresnel lens is acting as a focusing monochromator producing cylindrical wave front - a sagittally focused beam remains a very parallel in meridional plane. This focusing monochromator can be applied in high resolution diffraction technique: double- and triple-crystal diffractometry for a detailed study of nearly perfect semiconductor crystals with topological surface structure. High angular resolution can be easily achieved using an asymmetrically cut BFL crystal, so standing wave technique with lateral resolution of about 1μm is also feasible.

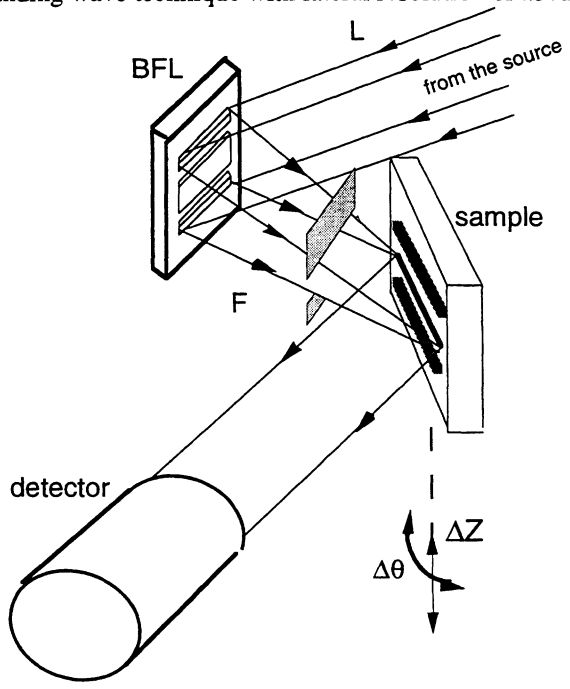

Fig. 8. The setup of the microfocus double crystal diffractometer

The microfocus X-ray diffraction measurements were carried out at the Optics beamline using a two axis of three-axis diffractometer in (+n, -n) setting consisting of a Si (111) Bragg-Fresnel lens and the sample (Fig.8.)[20]. The Si-111 Bragg reflection was set to select 12 keV radiation from bending magnet. A Huber slit was placed on the downstream side of the BFL to avoid the background radiation from the flat area of the Si substrate. A sample was located at the focal plane in 30 cm from BFL

Using this setup III/Y heterostructures grown by different selective area epitaxy techniques (planar and embedded selective area MOVPE and MOMBE) were investigated. The samples were test structures of InGaAs and InGaAsP layers grown on an InP (001) substrate that was partially masked with SiO_2 fields and laser/waveguide devices laterally integrated on an InP (001) wafer. In order to determine the lattice mismatch close to the boundaries of the layer / oxide and laser / waveguide boundary, rocking curve scans with micrometer step width were performed. The lattice distortions of the III/Y - heterostructures show changes at the boundaries in the range of 5 μm to 100 μm depending on the selected process.

3. MICROIMAGING

3.1. Beam emittance monitor

The application of the circular Si-based Bragg-Fresnel lenses (BFL) for X-ray undulator sources imaging in backscattering geometry has been proposed and realized on the ESRF Machine Diagnostics Beamline[21]. To measure the value of the emittance *in situ* a second optical element as an image expander has been applied in order to fit the resolution of 2D detector currently available (~30μm)[22,23]. Two optical geometry's have been tested at the energy 8keV. In a first setup the image formed by the long focus (F=1.25m) BFL as an objective lens has been vertically enlarged by asymmetrically reflected Si-422 crystal with magnification 15 that corresponds to asymmetry factor. The enlarged image was recorded by X-ray CCD camera having a resolution of 30 μm FWHM. In a second setup classical telescope geometry was applied when two BFLs were used in tandem. The first objective forms a real inverted image, which was examined using the second short focus BFL (F=0.25m), the eyepiece. The second focal plane of the objective nearly coincided with the first focal plane of the eyepiece and a 100μm pinhole was installed in this plane in order to spurs the zero diffraction order for better image contrast. The image was recorded by X-ray CCD placed at 1.5m distance from the second lens.The computer recorded images for both optical setups were treated and the deduced values of the emittance are in a good agreement with other estimates.

3.2. Phase contrast microscopy

Usual principle of the microscopy based on amplitude contrast which arises through differences in the absorption length from material to material. From this concept x-ray imaging microscopy is practically impossible for hard x-rays. It is well known that the contrast of the sample to be imaged can be enhanced considerably by using phase contrast. Zernicke type phase contrast microscopy was realised in soft x-ray domain. In principle the same approach can be apply for hard x-rays using BFO or zone plates. But we suggested to use another way. High level of collimation and coherency of the x-ray beam provided by the ESRF sources make it possible to develop phase sensitive technique[24-26]. The transmission X-ray microscope was tested at the High Brilliance beamline[27]. A test sample - a free-standing 0.5μm gold grating supported by the bigger mesh with 15μm pitch size and 3μm bar - was attached to a 70μm Pt pinhole. A torroidal mirror was used as a condenser to create the beam of about 50 μrad in convergence. Fine grid can be clearly seen not only in the open areas of the supporting mesh but also underneath the 3μm bars. The image contrast measured is significantly higher than it should be due to a simple absorption, that shows a phase nature of the image formation. Moreover depth of the image field was experimentally measured to be almost infinite, that confirms very coherent illumination optical setup like in laser microscopy.

3.4. Microtomography

Considering the small divergence and coherent properties of the beam evident benefits might be achieved in the development of phase contrast tomography. The first results on phase-contrast tomography were obtained at 50keV recently[28]. For phase contrast tomography with parallel illumination the resolution is determined by the resolution of the detector: at present this is 5-10 μm for high resolution X-ray cameras and 1 μm for high resolutions films. The use of additional optics like a Bragg-Fresnel lens installed after the object should lead to a 0.1 μm resolution.

7. APPENDIX. THEORY OF BRAGG-FRESNEL CRYSTAL OPTICS

Fig. 9. Experimental setup

The theory of the Bragg-Fresnel crystal optics is elaborated similar to the theory of Fresnel zone plate (FZP). On the first stage, one has to consider the spherical monochromatic x-ray wave incident on the BFL. On the second stage, the Bragg diffraction of the x-ray wave inside the perfect crystal or the crystal with specially modulated surface layer containing the Fresnel phase zone profile has to be taken into account. On the final third stage, the transfer of the field from BFL to the observation plane (2D detector) has to be considered. The reference coordinate systems on the source, BFL and 2D detector are shown in the Fig.9. Here we will consider two cases: (1) linear curved BFL with the Fresnel phase zone profile in a sagittal plane and the plane of diffraction scattering as a meridional plane; and (2) circular BFL with circular Fresnel zone profile in the backscattering diffraction geometry. The resultant wave field distribution at the plane of 2D detector may be written for both cases in the following general form

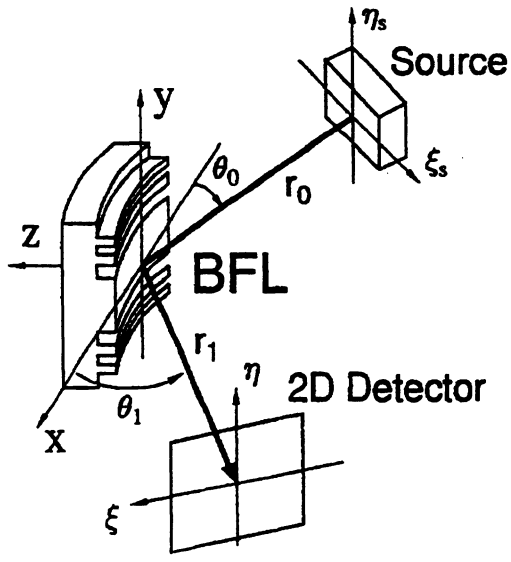

$$E(\xi,\eta) = E_0(\xi,\eta)\,[1 + P(\xi)Q(\xi,\eta)] \tag{1}$$

where

$$E_0(\xi,\eta) = \frac{F_{etch}(\xi)}{r}\exp\left(i\frac{2\pi}{\lambda}\left[r + \frac{1}{2r}[(\xi-\xi_s)^2 + (\eta-\eta_s)^2]\right]\right), \qquad r = r_0 + r_1 . \tag{2}$$

E_0 is the wave field of the spherical wave at the total distance from the source to the detector disturbed by the Bragg reflection process through the function F_{etch}. The function $P(\xi)$ describes the difference in the Bragg reflection processes by the etched and free parts of the surface region

$$P(\xi)=\frac{F_{free}(\xi)}{F_{etch}(\xi)}-1\ , \tag{3}$$

while the function $Q(\xi,\eta)$ describes the focusing of the field by the Fresnel phase zone profile similar to the theory of FZP. The functions F_{etch} , F_{free} and Q have different analytical form in the different cases considered.

So in the case 1 (linear curved BFL) one can obtain

$$F_{free}(\xi)=\frac{1}{2\pi\gamma_0}\left(\frac{i\lambda r}{M_0M_1}\right)^{\frac{1}{2}}\exp\left(-i\pi\frac{(\xi-\xi_s)^2}{\lambda r}\right)\times$$
$$\times\int dq\,R(q)\exp\left(i\frac{(\xi-\xi_s^i-\xi_\lambda)q}{\gamma_1M_1}-i\frac{\lambda r_m}{4\pi\gamma_1^2M_0M_1}q^2\right) \tag{4}$$

while $F_{etch}(\xi)$ differs from $F_{free}(\xi)$ by replacing ξ_s^i on $\xi_s^i+\xi_h$. The following notation is used

$$\gamma_{0,1}=\sin\theta_{0,1}\,,\quad c_{0,1}=\cos\theta_{0,1}\,,\quad M_{0,1}=1-\frac{r_{0,1}}{\gamma_{0,1}R_c}\,,\quad r_m=r_1M_0+r_0M_1\frac{\gamma_1^2}{\gamma_0^2}\,,$$
$$\xi_s^i=\xi_s\frac{\gamma_1M_1}{\gamma_0M_0}\,,\quad \xi_\lambda=\frac{\Delta\lambda}{\lambda}\left[r_1\frac{(c_1-c_0)}{\gamma_1}-r_m\frac{\gamma_0tg\theta_B}{\gamma_1M_0}\right],\quad \xi_h=M_1\frac{\sin2\theta_B}{\gamma_0}h\,. \tag{5}$$

It is assumed that the BFL is cylindrically bent with the radius of curvature R_c, h is the depth of BFL profile, while θ_B is the Bragg angle. The function $R(q)$ in Eq.(4) is the reflection amplitude of the plane wave by the crystal lattice of the lens. The plane wave has the wave vector which deviates from the Bragg condition by q where q is the component along the surface. In the case of perfect crystal this function is well known and the function $|R(q)|^2$ shows the well known Darwin curve in the reflectivity plot. However taking into account the crystall lattice deformation, for example, owing to elastical bending, this function have to be found as the solution of the Takagi equation with the given deformation profile. The function $Q(\eta)$ for the linear BFL does not depend on ξ and can be written in the form

$$Q(\eta)=\frac{\rho_f}{\sqrt{i\lambda r_1}}\sum_{\pm}\sum_{n=0}^{N-1}\int_{\sqrt{2n}}^{\sqrt{2n+1}}dt\,\exp\left(i\pi\frac{\rho_f^2}{\lambda r_r}\left[t\pm\frac{r_r}{r_1\rho_f}(\eta+\eta_s\frac{r_1}{r_0})\right]\right),\quad r_r=\frac{r_0r_1}{r} \tag{6}$$

while ρ_f is the halfwidth of the first Fresnel zone. The focus distance r_f of the lens for a plane wave focusing is $r_f=\rho_f^2/\lambda$. Here $N=N_z/2$ where N_z is total number of Fresnel zones in which the phase of the spherical wave changes on π .

It is well known that a very good focusing by curved crystal occurs when the points of the source and of the observation are placed at the Rowland circle. In our notation it corresponds to the conditions $M_0=0$ and $M_1=0$ simultaneously. But with the synchrotron radiation source it is very hard to fullfil this conditions for a symmetrical case of diffraction ($\gamma_0=\gamma_1$) owing to very large source to lens distance. Instead a simple meridional focusing condition (MFC) is formulated as $r_m=0$, namely

$$\frac{\gamma_0^2}{r_0}+\frac{\gamma_1^2}{r_1}=\frac{\gamma_0+\gamma_1}{R_c} \tag{7}$$

Bragg-Fresnel lens works quite different in the cases when MFC is met or it is not met. If the MFC is not met then it is possible to consider the ray-approximation. The ray-approximation can be obtained by the Statianary Phase Method of the integral calculation. In this case the function $F_{free}(\xi)$ has an approximate analytical expression

$$F_{free}(\xi)=\frac{\gamma_1}{\gamma_0}\sqrt{\frac{r}{r_m}}R(q_s)\exp\left(i\pi\left[\frac{M_0(\xi-\xi_s^i-\xi_\lambda)^2}{M_1\lambda r_m}-\frac{(\xi-\xi_s)^2}{\lambda r}\right]\right) \tag{8}$$

The phase shift of the Fresnel structure under the condition $\xi_s^i=\xi_\lambda=0$ can be determined now as following

$$\varphi_0(\xi)=\frac{\pi M_0}{M_1\lambda r_m}\left[\xi^2-(\xi-\xi_h)^2\right]\approx\frac{2\pi M_0\gamma}{\gamma_0\lambda r_m}\xi h \tag{9}$$

On the other hand the reflectivity is determined by the parameter

$$q_s=\frac{2\pi\gamma_1 M_0}{\lambda r_m}\xi \tag{10}$$

These formulas show that both the phase shift and the reflectivity depent on ξ. The condition of coincidence the equality $\varphi_0=-\pi$ with the maximum of reflectivity can be obtained as the condition on the height of etching

$$h=h_0=\frac{\lambda\gamma_0\gamma_1}{|\chi_{0r}|(\gamma_0+\gamma_1)} \tag{11}$$

It is interesting that this condition does not depend on R_c. It is possible to obtain the correspondence between the point on the lens *(x)* and on the detection plane *(ξ)* through the angular deviations from the reference direction defined by the vector $\mathbf{k}_1=\mathbf{k}_0+\mathbf{h}$, where **h** is the reciprocal lattice vector (the diffraction vector). This dependence *ξ(x)* shows the ray distribution where x is the beginning of the ray and ξ is the end.

When MFC is met *(r_m=0)* all rays have the same end because ξ does not depend on x. The point of meridional focusing ξ_f is determined by the next expression

$$\xi_f=\xi_\lambda+\xi_s^i \qquad \text{with} \quad \xi_\lambda=\frac{\Delta\lambda}{\lambda}\frac{(c_1-c_0)}{\gamma_1}, \qquad \xi_s^i=\xi_s\frac{\gamma_0 r_1}{\gamma_1 r_0}. \tag{12}$$

In this case the image of the point source in a meridional direction is described in accordance with (4) by the Fourier transform of the reflectivity amplitude which determines the size of the focus spot. The Eq.(8) is not valid now. The displacement owing to etching is comparable with the size of focus. It means that etched part of the surface gives the image of the point source in the different place and as a consequence the focusing in a sagittal plane takes the properties of amplitude Fresnel zone plate together with the phase one depending on the relation between the size of focus spot and ξ_h. .

In the case 2 (the circular lens in a backscattering geometry) the Bragg diffraction allows to reflect the beam in back direction but does not influence the focusing properties which stay the same as for the circular Fresnel zone plate (FZP). The reflection occurs only for the definite wavelength of the radiation and inside the narrow wavelength band the width of which is determined by the width of the total reflection region (Darwin width). The formulas (1) to (3) are valid in this case too but $F_{free}=R_{free}$ is simply the reflection amplitude which does not depend on ξ while $F_{etch}=R_{etch}$ is the same for the etched part of the crystal. The reflection amplitude R_{free} and R_{etch} in the case of perfect crystal is determined by well known expressions

$$R_{free}=\chi_h^{-1}\left[-\chi_0+2\delta\pm\sqrt{(-\chi_0+2\delta)^2-\chi_h^2}\right], \quad R_{etch}=R_{free}\exp\left(-4\pi i\frac{h}{\lambda}\delta\right). \tag{13}$$

where $\delta=\Delta\lambda/\lambda$ is the relative wavelength shift from the reference value which corresponds to the kinematical Bragg diffraction condition. According to this formula the reflectivity of the Bragg-Fresnel lens is limited by the narrow wavelength band with the centre in $\delta=-|\chi_{0r}|/2$ and the width $|\chi_{hr}|/2$. On the other hand, the phase shift depends on the depth of etching h as well as on δ directly proportionally. The optimum value of the depth of etching h follows from the condition that the phase has to be equal $-\pi$ at the centre of Darwin table. In this way we obtain $h=\lambda/2|\chi_{0r}|$.

As for the function Q it is determined by the following integral with a use of cylindrical coordinates

$$Q=\frac{\rho_f^2}{i\lambda r_r}\sum_{n=0}^{N-1}\int_{\sqrt{2n}}^{\sqrt{2n+1}}dt\,t\int_{-\pi}^{\pi}d\varphi\exp\left(i\pi\frac{\rho_f^2}{\lambda r_r}\Phi(t,\varphi)\right), \tag{14}$$

$$\Phi(t,\varphi)=t^2+t_1^2+t_0^2-2tt_1\cos\varphi-2tt_0\cos(\varphi+\Delta\varphi)+2t_0t_1\cos\Delta\varphi$$

where ρ_f is the radius of the first Fresnel zone and the following notation is used

$$(\xi_s,\eta_s)\to(\rho_0,\varphi_0),\quad (\xi,\eta)\to(\rho_1,\varphi_1),\quad (x,y)\to(\rho,\varphi),$$
$$t=\frac{\rho}{\rho_f},\quad t_0=\rho_0\frac{r_r}{r_0\rho_f},\quad t_1=\rho_1\frac{r_r}{r_1\rho_f},\quad \Delta\varphi=\varphi_1-\varphi_0 \tag{15}$$

It is easy to see from this expression that if the source lies at the central axis of the lens ($\rho_0=0$) then the intensity distribution has an axial symmetry, i.e. the dependence on $\Delta\varphi$ vanishes. If the source deviates from the axis then the angle between polar directions of source and observation points is essential. The focusing takes place at the point which lies at the line passing through the source point and the centre of the lens from the opposite side, i.e when $\Delta\varphi=\pi$. In this case the function Q takes the form

$$Q(\xi,\eta)=2\pi\frac{\rho_f^2}{i\lambda r_r}\exp\left(i\pi\frac{(\rho_f a)^2}{\lambda r_r}\right)\sum_{n=0}^{N-1}\int_{\sqrt{2n}}^{\sqrt{2n+1}}dt\,t\,J_0(bt)\exp\left(i\pi\frac{(\rho_f t)^2}{\lambda r_r}\right),$$
$$a=t_1-t_0\frac{r_1}{r_0}=\frac{r_r}{r_1\rho_f}\left(\rho_1-\rho_0\frac{r_1}{r_0}\right),\qquad b=2\pi\frac{\rho_f^2}{\lambda r_r}a \tag{16}$$

Here J_0 (z) is the Bessel function of zero order. According to this formula when the source point deviates from the axis the focus point is also deviated in the opposite direction on the distance which differs from the source deviation distance on the magnification factor r_1/r_0. In this direction the size of focus spot is the same for any value of deviation (in the limits of validity of the small angle approximation). The maximum intensity at the focus can be estimated in this case explicitly. Indeed, $P=-2$, the function Q equals $2N$ when $a=0$ and we have the estimation $I_{foc}=16N^2=4N_z^2$ for the intensity at the focus.

The formula (16) is written for the focusing of the fisrt order when the phase changes on 2π inside the each two zones (so called the unit cell of the lens) and the integral is taken over the half of the unit cell (simple structure). The analogous expressions can be written for the focusing of nth order when the phase changes on $2\pi n$ inside one unit cell and an integration is performed only over the free part of the cell. If this part equals to a part of cell with the phase change πn then only the odd orders lead to focusing. But here is another possibility when the size of free part of cell corresponds to a phase change π for all cases but the size of etched part of cell corresponds to a phase change $\pi(2n-1)$. In this case the focusing is possible for all orders. On the other hand, this way gives the maximum width of etched part of cell which is very important from the point of view of the BFL fabrication.. We want to notice that the estimation $I_{foc}=16N^2$ where N is a number of the cells is valid for the complicated BFL which contains the cells of different orders. Only the total number of cells is essential. Naturally the structure of the focus spot will depend on the structure of the BFL.

Another problem of circular BFL is a very narrow energy band of focused radiation. There is two ways to improve the properties of the BFL. First one is to eliminate the energy dependence of the phase shift by the etched regions. Second one is to make the reflectivity curve more wide in the energy space. The practical realisation of these ways consists of the use of the perfect crystals with the specially deformed subsurface layer in the direction normal to the surface. As is well known from the dynamical theory of X-ray diffraction in deformed crystals, in this case the reflection amplitude is determined from the Takagi equation which takes the next form for the case of back-scattering geometry

$$\frac{dR}{dz}=\frac{2\pi i}{\lambda}\left[\left(-\chi_0+2\delta+2\frac{\Delta d}{d}\right)R-\frac{1}{2}\chi_h(1+R^2)\right] \tag{17}$$

where $\Delta d/d$ is depending on z relative change of the lattice spacing in z-direction which is normal to the surface. In this way R_{free} and R_{etch} must be determined from (17) separately.

9. REFERENCES.

1. V.V.Aristov, A.A.Snigirev, Yu.A.Basov, A.Yu.Nikulin, "X-ray Bragg optics", AIP Conf. Proc., 147, pp. 253-259, 1986.

2. V.V.Aristov, Yu.A.Basov, S.V.Redkin, A.A.Snigirev, V.A.Yunkin, "Bragg zone plates for hard X-ray focusing", Nucl.Instrum.& Methods A261, pp. 72-74, 1987.

3. V.V.Aristov, Yu.A.Basov, G.N.Kulipanov, V.F.Pendyurin, A.A.Snigirev, A.S.Sokolov, "Focusing properties of a Bragg-Fresnel lens in a white spectrum of synchrotron radiation", Nucl. Instrum.& Methods A274, pp. 390-393, 1989.

4. V.V.Aristov, Yu.A.Basov, A.A.Snigirev, "Synchrotron radiation focusing by a Bragg-Fresnel lens" Rev. Sci. Instrum., 60, pp. 1517-1518,1989.

5. V.Aristov, S.Kuznetsov, A.Snigirev, "The computer-aided design of the hard X-ray diffraction lenses", Inst. Phys. Conf. Ser. No130, pp. 543-546, 1992.

6. E.Aristova. C.David, A.Freund, Ya.Hartman, B.Kaulich, A.Snigirev, V.Yunkin, Phase Circular Bragg-Fresnel Lens Based on Germanium Single Crystal", Proc. of 4-th International Conference on X-Ray Microscopy, September 1993, Chernogolovka, Russia, to be published in X-ray Microscopy IY, 1995.

7. V.V.Aristov, Yu.A.Basov, A.A.Snigirev, V.A.Yunkin, "Bragg-Fresnel lens with the slope zone structure", Rev. Sci. Instrum., 63, pp. 586-587, 1992.

8. V.V.Aristov, Yu.A.Basov, T.E.Goureev, A.A.Snigirev, T.Ischikawa, K.Izumi, S.Kikuta, "Focusing properties of a linear-phase Bragg-Fresnel lens", Jpn. J. Appl. Phys., vol.31, pp. 2616-2620, 1992.

9. Yu.A.Basov, T.L.Pravdivtseva, A.A.Snigirev, M.Belakhovsky, P.Dhez, A.Freund, "Two dimensional focusing of hard X-rays by a phase circular Bragg-Fresnel lens in the case of the Bragg backscattering", Nucl. Instrum.& Methods A308, pp. 363-366, 1991.

10. U.Bonse, C.Riekel, A.A.Snigirev, "Kirkpatrick-Baez microprobe on the basis of two linear single crystal Bragg-Fresnel lenses", Rev. Sci. Instrum.,63, pp. 622-624, 1992.

11. V.V.Aristov, Yu.A.Basov, Ya.M.Hartman, A.A.Snigirev, C.Riekel, "X-ray microprobes based on Bragg-Fresnel crystal optics for high energy X-rays", Inst. Phys. Conf. Ser. No130, pp. 523-526, 1992.

12. Ya.Hartman, A.Freund, I.Snigireva, A.Snigirev, "Two-dimensional X-ray focusing using curved linear Bragg-Fresnel Lens", to be published.

13. A.Snigirev, "The Recent Development of Bragg-Fresnel Optics. Experiments and Applications at the ESRF", Rev. Sci. Instr, 66(2), pp. 2053-2058, February 1995.

14. H.Chanzy, C.Riekel, I.I.Snigireva, A.A.Snigirev, "BFL-Based Hard X-Ray Microprobe for Microdiffraction. Some Aspects of Sample Preparation and Sample Alignment", Proc. of 4-th International Conference on X-Ray Microscopy, September 1993, Chernogolovka, Russia, to be published in X-ray Microscopy IY, 1995

15. S.M.Kuznetsov, I.I.Snigireva, A.A.Snigirev, P.Engström, C.Riekel, "Sub-micrometer Fluorescence Microprobe Based on Bragg-Fresnel Optics", Appl.Phys.Lett. 65 No 7, pp. 827-829, 15 August, 1994.

16. A.Snigirev, I.Snigireva, P.Engström, S.Lequien, A.Suvorov, Ya. Hartmann, P.Chevallier, F.Legrand, G.Soullie, M.Idir, "Testing of Sub-Micrometer Fluorescence Microprobe Based on Bragg-Fresnel Crystal Optics at the ESRF", Rev. Sci. Instr., 66(2), pp.1461-1463, February 1995.

17. P.Chevallier, P.Dehz, F.Legrand, M.Idir, G.Soullie, A.Mirone, A.Erko. A.Snigirev, I.Snigireva, A.Suvorov, A.Freund, P.Engstrom, J.Als Nielson, A.Grubel, "First test of the scanning X-ray microprobe with Bragg-Fresnel multilayer lens at ESRF beam line", Nucl. Instrum.& Methods, A354,pp. 584-587, 1995.

18. A.A.Snigirev, I.I.Snigireva, C.Riekel, A.Miller, L.Wess, T.Wess, "A Double Focusing Camera with mm Focal Spot Based on a Circular Bragg-Fresnel Lens", Journal de Physique IV, Vol.3, C8,Suppl.JP III, N12, pp. 443-446, 1993.

19. M.Hanfland, D.Hausermann, A.snigirev, I.Snigireva, Y.Ahahama, M.Mcmahon, "Bragg-Fresnel Lens for high pressure studies, ESRF Newsletters, No22, pp. 8-9, November 1994.

20. A.Iberl, M.Schuster, H.Göbel, B.Baur, R.Matz, A.Snigirev, I.Snigireva, A.Freund, B.Lengeler, H.Heinecke, "Microfocus double crystal X-ray diffractometry on III/Y- heterostructures grown by selective area epitaxy", J. Phys. D: Appl. Phys., 28, pp. A200-A205, 1995.

21. E.Tarasona, P.Elleaume, J.Chavanne, Ya.M.Hartman, A.A.Snigirev, I.I.Snigireva, "2D Imaging of an Undulator Source by Phase Circular Bragg-Fresnel Lens", Rev. Sci. Instr., 65(6), pp. 1959-1963, 1994

22. Ya.Hartman, E.Tarazona, P.Elleaume, I.Snigireva, A.Snigirev, "Imaging of an undulator source by phase circular Bragg-Fresnel lenses", Journal de Physique IY, Colloq.C9, vol.4, pp. C945-C948, 1994.

23. Ya.Hartman, E.Tarazona, P.Elleaume, I.Snigireva, A.Snigirev, "Emittance monitors based on Bragg-Frsnel lenses", Rev. Sci. Instrum., 66(2),pp. 1978-1980, February 1995.

24. A.Snigirev, I.Snigireva, A.Suvorov, M.Kocsis, V.Kohn, "Phase contrast imaging by coherent high energy synchrotron radiation", ESRF Newsletters, No24, pp. 23-25, June 1995.

25. A.Snigirev, I.Snigireva, V.Kohn, S.Kuznetsov, I.Schelokov,"On the possibilities of X-ray phase contrast imaging by coherent high energy synchrotron radiation", to be published in Rev. Sci. Instrum..

26. A.Snigirev, I.Snigireva, V.Kohn, S.Kuznetsov, "On the requirements to the instrumentation for the new generation of the synchrotron radiation souces. Beryllium windows", to be published in Nucl. Instrum. & Methods.

27. A.Snigirev, I.Snigireva, P.Bösecke, S.Lequien, "Phase contrast imaging microscopy at 10 keV energy using circular Bragg-Fresnel Lens", to be published

28. C.Raven, A.Snigirev, I.Snigireva, P.Spanne, A.Suvorov, "Diffraction Microtomography with 50keV X-ray Synchrotron Radiation", to be published.